JOURNAL OF GEOPHYSICAL RESEARCH, VOL. 104, NO. D13, PAGES 16,419–16,435, D20, 1999

Three-dimensional simulation of stratospheric trace gas distributions measured by CRISTA

M. Riese
Physics Department, University of Wuppertal, Wuppertal, Germany

X. Tie and G. Brasseur
National Center for Atmospheric Research, Boulder, Colorado

D. Offermann
Physics Department, University of Wuppertal, Wuppertal, Germany

Abstract. The Cryogenic Infrared Spectrometers and Telescopes for the Atmosphere (CRISTA) experiment has been flown on two space shuttle missions (STS 66 and STS 85). During these missions, global trace gas distributions have been measured with high spatial resolution. The first flight was performed in early November 1994 during a period of disturbed dynamical conditions characterized by relatively large wave activity and associated exchange of tropical and extratropical air. As a result, numerous small- and medium-scale structures were present in the trace gas distributions measured by CRISTA. The detailed structure of the constituent distributions has been modeled with the National Center for Atmospheric Research Research on Ozone in the Stratosphere and Its Evolution (ROSE) model, which is driven by assimilated winds and temperatures provided by the U.K. Meteorological Office. The modeled trace gas distributions capture much of the measured structures. Very good agreement is found in the lower stratosphere of the northern hemisphere, with the exception of unrealisticly high variability of the modeled trace gas fields at equatorial and subtropical latitudes. In this paper, model results of two specific tracers, CFC-11 and N_2O, are compared to respective CRISTA measurements. For quantitative comparisons of trace gas transport in the ROSE model and trace gas transport associated with the measurements, CRISTA version 1 (level 2) data have been assimilated into the model by using a simple sequential technique. The trace gas assimilation system interpolated the measured distributions of long-lived tracers onto the model grid and yields synoptic fields that are consistent with the CRISTA measurements, at each time step of the model (20 min). Horizontal eddy fluxes of CFC-11 (31.6 mbar) calculated from the assimilated trace gas concentrations are in reasonable agreement with respective fluxes calculated from modeled trace gas fields without data assimilation. Both data sets indicate a large degree of temporal cancellation of eddy transport during the time period of the CRISTA measurements. The assimilated trace gas distributions represent a value-added level 3 product, which has been used for transport and budget studies of CFC-11 (31.6 mbar) and CH_4 (4.6 mbar). The study indicates that irreversible transport processes are rather important at the 4.6 mbar pressure level during the time period of the CRISTA measurements. Most interesting is a pronounced mixing event from midlatitudes into the tropics, which is also evident in measured and calculated zonal mean CH_4 mixing ratio tendencies.

1. Introduction

Atmospheric minor constituents such as nitrous oxide (N_2O), methane (CH_4), and chlorofluorocarbons (CFCs) are valuable tracers of stratospheric air motions. Satellite and aircraft observations of N_2O and CH_4 have been used in numerous studies of the stratospheric circulation and of stratospheric transport and mixing processes [e.g., *Mahlmann et al.*, 1986; *Solomon et al.*, 1986; *Holton and Choi*, 1988; *Garcia et al.*, 1992; *Schoeberl et al.*, 1992; *Randel et al.*, 1993, 1994; *Stanford et al.*, 1993; *Kindler et al.*, 1998]. The Cryogenic Infrared Spectrometers and Telescopes for the Atmosphere (CRISTA) experiment [*Offermann et al.*, this issue] provides global distributions of atmospheric trace gases (including N_2O, CH_4, and CFC-11) in the stratosphere with high horizontal resolution (typically 6° in longitude and 3° in latitude). The CRISTA data are especially suited to study small- and medium-scale dynamical and photochemical structures associated, for example, with planetary wave breaking [e.g., *McIntyre and Palmer*, 1983] or tropical/extratropical exchange of air by planetary wave mixing events [e.g., *Randel et al.*, 1993].

CRISTA has been flown on two space shuttle missions (STS 66 and STS 85). In this paper, trace gas concentrations from the first flight in early November 1994, which was part of the Atmospheric Laboratory for Applications and Science 3 (ATLAS 3) mission of NASA [see *Kaye and Miller*, 1996], are

Paper number 1999JD900178.
0148-0227/99/1999JD900178$09.00

analyzed. The meteorological conditions prevalent during the ATLAS 3 mission have been described by *Manney et al.* [1996] and by *Naujokat and Pawson* [1996]. During the flight the north polar vortex had started to build up, while the south polar vortex had started to decay. The north polar vortex had developed above 35 mbar. The south polar vortex was strong below 16 mbar with coherent fragments up to 3 mbar. The situation was further characterized by enhanced temporal variability and strong small-scale and medium-scale dynamical structures. For example, several streamers of tropical and arctic air have been found in the CRISTA measurements [e.g., *Offermann et al.*, this issue; *Bacmeister et al.*, this issue; *Riese et al.*, 1997, this issue]. The northern hemispheric streamers of a specific day and altitude (November 6, 27 km) have been reproduced by *Kouker et al.* [this issue] in an idealized tracer study. Analyses of high-resolution potential vorticity (PV) fields generated by reverse trajectory calculations [*Manney et al.*, 1996] also indicate that low-latitude air was drawn around both vortices almost continuously. In addition, air was drawn off the vortices, leading to very complex air motions, especially over the Pacific Ocean and the western United States.

High-resolution distributions as measured by CRISTA are ideally suited for studying such disturbed dynamical conditions, especially when they are used in conjunction with a three-dimensional chemical transport model (CTM). In this paper, CRISTA version 1 (V1) trace gas distributions are compared and combined with the National Center for Atmospheric Research (NCAR) Research on Ozone in the Stratosphere and Its Evolution (ROSE) model. In this study the ROSE CTM is driven by assimilated winds and temperatures provided by the United Kingdom Meteorological Office (UKMO), and contains a detailed photochemical scheme (see section 3). However, the results presented in sections 3 to 6 are not sensitive to photochemical processes, since they focus on long-lived tracers measured by CRISTA.

Assimilated winds provided by the U.K. Meteorological Office or the NASA Goddard Space Flight Center (GSFC) data assimilation system (GEOS1DAS) [*Suarez et al.*, 1995] have been widely used for transport studies of atmospheric trace constituents [e.g., *Rood et al.*, 1989, 1992; *Rosenlof and Holton*, 1993; *Chen et al.*, 1994; *Douglass et al.*, 1996]. Horizontal wind distributions produce synoptic variations in trace gas fields (e.g., of N_2O) which compare relatively well with instantaneous trace gas measurements. However, there is also evidence for some limitations in using the assimilated horizontal wind fields. For example, isentropic mixing rates are too large in the subtropics [e.g., *Kindler et al.*, 1998; *Chipperfield*, 1999]. Thus the high horizontal resolution of the CRISTA trace gas measurements provides a critical test of the ability of assimilated winds to produce accurate instantaneous synoptic maps.

In this paper, distributions of nitrous oxide (N_2O) and chlorofluorocarbon (CFC-11) measured by CRISTA are compared to model calculations. As will be shown in sections 3, 4, and 5, the model captures much of the measured structures. However, some limitations apply, especially in the southern hemisphere and at high altitudes (above 10 mbar).

For quantitative analyses of trace gas transport and mixing processes, a simple trace gas assimilation technique has been developed in order to combine CRISTA measurements with constituent fields derived by the ROSE CTM (see section 5). In the case of long-lived tracers, the CTM is rapidly forced toward the observations, and the UKMO winds essentially provide temporal and spatial interpolations (and extrapolations) of the measured concentrations. This way, the assimilation system provides synoptic trace gas maps, which are consistent with the asynoptic CRISTA measurements. These maps are hereafter referred to as "analyzed maps." Analyzed maps of CFC-11, N_2O, and CH_4 are shown and discussed in sections 5 and 6. Horizontal CFC-11 fluxes (31.6 mbar) associated with the analyzed CRISTA observations and with the UKMO meteorological data are compared to fluxes derived from model results without trace gas assimilation. In addition, analyzed CH_4 fields (4.6 mbar) are used to derive mixing ratio tendencies associated with strong irreversible mixing processes that occurred during the measurement period of CRISTA.

2. Data Description

Trace gas distributions used for this study are taken from the first CRISTA flight, which took place in early November 1994. CRISTA uses the limb sounding technique to measure infrared emissions of various trace gases in the middle atmosphere [*Offermann et al.*, this issue]. This technique yields a dense horizontal (see Plate 1) and vertical measurement net (see Table 1), and it allows measurements during nighttime and daytime. The instrument is mounted on the CRISTA-SPAS satellite which is released from the space shuttle and operates at a distance of 50–100 km behind it. Measurements with unprecedented horizontal resolution (for a limb sounding instrument) are taken during a free-flying period of about 1 week. The high horizontal data density is achieved by using three telescopes simultaneously. High measuring speed is achieved by cooling the optics and the infrared detectors with cryogenic helium.

During the first mission, about 50,000 height profiles of trace gas emissions were measured from a 300 km, 57° inclination orbit by using a number of different measurement modes (Table 1). Observations are available for the time period from November 4–12, 1994 (day 308/1735 to day 316/1045). The latitudinal coverage of the observations of the first mission is from −57° to +67°. A description of the data processing and the version 1 (V1) retrieval of atmospheric temperatures and trace gas mixing ratios is given by *Riese et al.* [this issue]. The version 1 retrieval includes CFC-11, N_2O, CH_4, HNO_3, N_2O_5, $ClONO_2$, and ozone. Table 2 shows random errors of the CRISTA version 1 data sets.

A global map of retrieved CFC-11 mixing ratios (21 km) is shown in Plate 1. The distribution was measured on November 7 using the stratospheric measurement mode (Table 1). The measuring tracks of the three telescopes can easily be identified. Each colored symbol represents a vertical CFC-11 profile with an altitude step of 1.5 km. The horizontal distance of two adjacent measurement points is about 200 km along the flight track (in this measurement mode) and about 600 km across the flight track. At the northern and southern turning point of the orbital track a complete coverage of a latitudinal circle takes about 24 hours, and all measurements are obtained at about the same local time. At the equator a complete coverage takes only 12 hours since the ascending and the descending nodes are separated by about 180° (12 hours in local time).

For this study, CRISTA V1 level 2 trace gas concentrations (instrument sampling grid) have been interpolated onto Upper Atmosphere Research Satellite (UARS) [*Reber*, 1985] pressure levels, which are also used by the CTM since the assimilated winds and temperatures are provided at these levels. The interpolated CRISTA data set has been used for the model

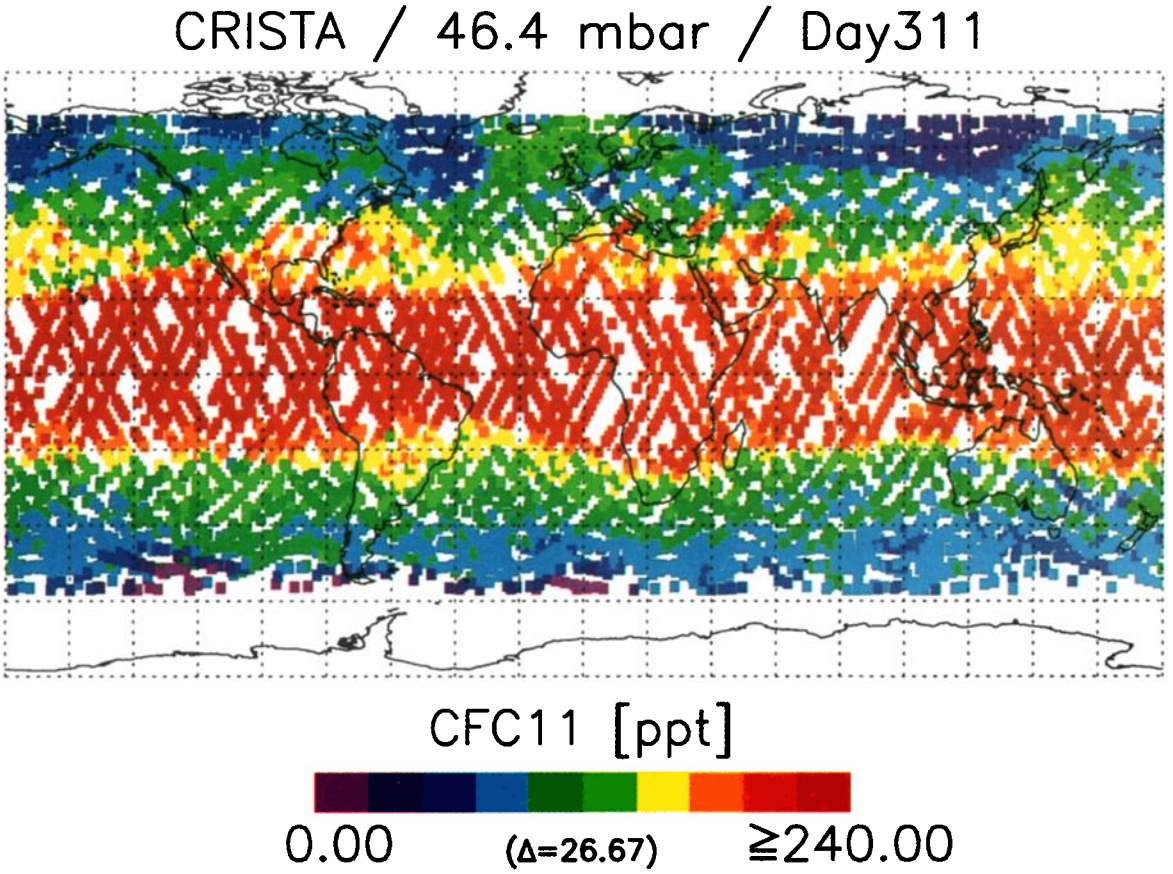

Plate 1. CFC-11 mixing ratios measured by CRISTA on November 7, 1994, at 46.4 mbar (21 km). The measurements were taken by using measurement mode 2 (see Table 1). The map shown in this figure covers longitudes from −180° to +180°E and latitudes from −80° to +80°.

initialization (see section 3.2) as well as for a trace gas assimilation system (see section 5). Since this analysis focuses on dynamical processes, modeled distributions of CFC-11 and N_2O are compared to respective measurements. Comparisons at and around 20 km focus on CFC-11 because CFC-11 data are of high quality in this region (the error of retrieved CFC-11 concentrations strongly increases with altitude; see *Riese et al.* [this issue]). Above 25 km, nitrous oxide is used, supplemented by observations of methane.

As described above, CRISTA measures with three telescopes (viewing directions) simultaneously. Version 1 trace gas data exhibit systematic differences between the three viewing directions of the order of 5 to 10%. For this study, the values of the lateral telescopes have been adjusted to the values of the center telescope by using mean differences calculated for the latitudinal band from −40° to +40° [see also *Riese et al.*, this issue].

3. Model Description

3.1. UKMO Wind-Driven ROSE Model

The three-dimensional ROSE model has been used for several previous studies of the middle atmosphere [see, e.g., *Rose*,

Table 1. CRISTA 1 Measurement Modes

Mode ID	Objective	Altitude Range*, km	Vertical Step*, km	Step Along Track*, kms	Hours of Data
1	stratosphere/mesosphere	16–79	1.5	400	54.6
2	stratosphere	16–44	1.5	200	76.7
M/T	mesosphere/lower thermosphere	60–164	2.7	360	4.3
V/R1	calibration	16–79	1.5	720	5
V/R2	calibration	16–44	3.0	190	5
H/O	oversampling	22–35	0.75	200	15
Total					160.6

*High-altitude scans [see *Riese et al.*, this issue] are not listed in this table. The vertical distance between two measurement points is denoted as "vertical step." The "step along track" indicates the distance between two subsequent altitude scans.

Table 2. Random Errors of CRISTA Version 1 Trace Gas Data

Trace Gas	Altitude Level, km					
	20	25	30	35	40	55
O_3	0.1 ppm	4.0%	4.3%	4.5%	4.2%	8%
$ClONO_2$	10%	6%	6%	7%		
CH_4		12%	8.5%	8.5%	7.5%	7.5%
N_2O		3%	3.5%	6.5%	7.5%	
N_2O_5			5%	5%		
CFC11	2.5%	2.5%				
HNO_3	3.8%	2.7%	2.3%			

1983; *Rose and Brasseur*, 1989; *Granier and Brasseur*, 1991; *Smith*, 1995]. In these studies, the model calculates "on line" the dynamical variables of the atmosphere (e.g., wind and temperature above 300 mbar). In the present study, the model version is driven "off-line" by analyzed winds and temperatures provided by the U.K. Meteorological Office (UKMO) [see also *Lefèvre et al.*, 1994].

The wind and temperature values are a product of a data assimilation system developed at the U.K. Meteorological Office [*Swinbank and O'Neill*, 1994] for the UARS project. The system assimilates a heterogeneous set of satellite temperature measurements and radiosonde observations into a global circulation model (GCM) in order to obtain self-consistent synoptic wind and temperature distributions at a specific time. Assimilated winds and temperatures are available for 22 pressure levels from the ground up to 0.316 mbar (55 km) with a vertical step of 2.7 km. This vertical step is of the order of the vertical resolution of CRISTA V1 trace gas data (2.5 to 3 km). The ROSE CTM uses 19 pressure levels between 316 mbar (8 km) and 0.316 mbar (55 km). The horizontal resolution of the meteorological data provided by the UKMO is 3.75° in longitude and 2.5° in latitude. This corresponds to 96 × 72 grid points for a given pressure level. Model runs with the CTM can be performed at this particular horizontal resolution or at somewhat lower horizontal resolutions (64 × 72, 32 × 36). The present study uses 64 × 72 grid points (5.65° in longitude and 2.5° in latitude).

The ROSE model accounts for the chemistry of oxygen, hydrogen, carbon, nitrogen, chlorine, and bromine species. About 100 gas phase reactions and seven heterogeneous reactions on volcanic aerosols and polar stratospheric clouds are included in the model. The reaction rate constants and absorption cross sections are taken from *DeMore et al.* [1994]. Solar irradiances are obtained from the Solar Stellar Irradiance Comparison Experiment (SOLSTICE) on board UARS. Photolysis rates are derived from precalculated lookup tables as a function of altitude, albedo, ozone column, and solar zenith angle. The chemical compounds are divided into two groups. Twenty-seven long-lived species (or families) are affected by both transport and chemistry. Fourteen short-lived or equilibrium species are calculated at each time step (20 min) neglecting transport. The transport of long-lived species and families is calculated with a semi-Lagrangian transport algorithm [*Smolarkiewicz and Rasch*, 1991]. Chemical species are transported along trajectories that are calculated every 5 min (in this study).

3.2. Model Initialization and N_2O Results at 14.7 mbar

In a first approach the model has been initialized by zonally symmetric trace gas fields which combine zonal mean CRISTA concentrations with results from the NCAR two-dimensional (2-D) chemical model [*Brasseur et al.*, 1990]. For this purpose, version 1 data of CFC-11, N_2O, CH_4, HNO_3, N_2O_5, $ClONO_2$, and ozone have been used. The initial concentrations of the nitrogen and chlorine families (and of all their members) were adjusted according to CRISTA measurements of HNO_3 and $ClONO_2$ by using the relative partitioning ratios of the family members given by the 2-D model results.

The initial trace gas fields are mainly based on CRISTA observations. Zonal averages of CRISTA values have been used in the latitudinal band from about −55° to +65°. The CRISTA values have been extrapolated to high northern and southern latitudes by means of latitudinal gradient information provided by the 2-D model. Vertical gradient information and lower boundary values of the 2-D model have been used to extrapolate the CRISTA values toward altitudes, where no observations are available.

This initialization has been improved at selected pressure levels by correlating concentrations of long-lived tracers measured by CRISTA with the potential vorticity (PV) derived from the UKMO data [see also *Lary et al.*, 1995]. At each pressure level the coefficients of a linear fit have been used to describe the relationship between PV and a given long-lived tracer. Only northern hemispheric values have been used; thus the absolute values of the initial trace gas distributions are somewhat tuned toward the conditions encountered in the northern hemisphere. In general, close correlations were found. Correlation coefficients are typically of the order of 0.8. The initial distributions of long-lived tracers have been calculated from the PV fields using the parameters from the linear fits. Through this approach, initial structures are introduced into the trace gas fields that exactly resemble the structures of the PV fields. No information about structures in the constituent fields observed by CRISTA enters the initialization. The model results presented in this paper are based on this initialization, which was applied to the model on November 1.

A comparison of a measured northern hemispheric N_2O distribution (14.7 mbar) with results obtained from the model is shown in Plate 2a for November 6 (day 310). The measurements were taken between day 309:12 and day 310:12, while the modeled distribution represents a synoptic map of day 310:0. The general shape of the polar vortex is well reproduced by the model. The associated wind field advects air out of the tropics toward higher latitudes. Two pronounced tropical extrusions can be seen in the CRISTA observations: one extrusion extends across the southern United States into the Atlantic Ocean, and the other extends along the North American and Asian Pacific coast. Air is also drawn off the vortex (e.g., south of the Atlantic extrusion). In addition, a very pronounced extrusion of Arctic air is drawn from Canada into the Pacific Ocean. The interaction of this Arctic extrusion with the Asian tropical extrusion results in very complex air motions, especially over the Pacific Ocean.

The model captures the Atlantic extrusion of tropical air and the Artic extrusion south of it. However, the strength of the Asian extrusion of tropical air and the associated transport along the coasts of Asia and North America are somewhat underestimated. For more quantitative comparisons of measured and the modeled structures, the N_2O values have been "detrended" by subtracting zonal mean values at each latitude (see Plate 2a). Through this approach, the synoptic structures of the N_2O fields are more emphasized, for example, the modeled Asian extrusion of tropical air. In general, synoptic struc-

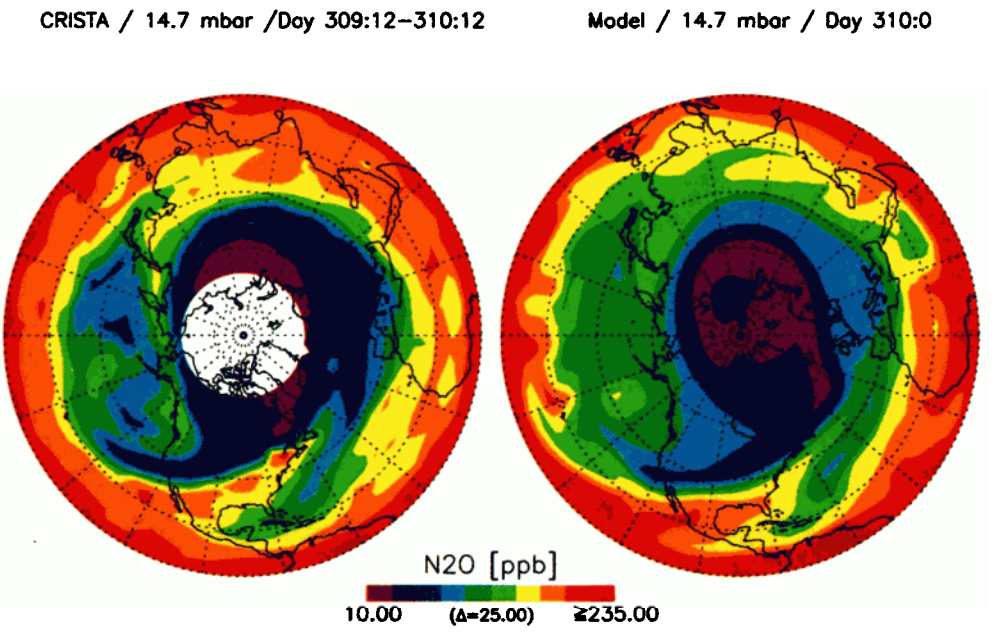

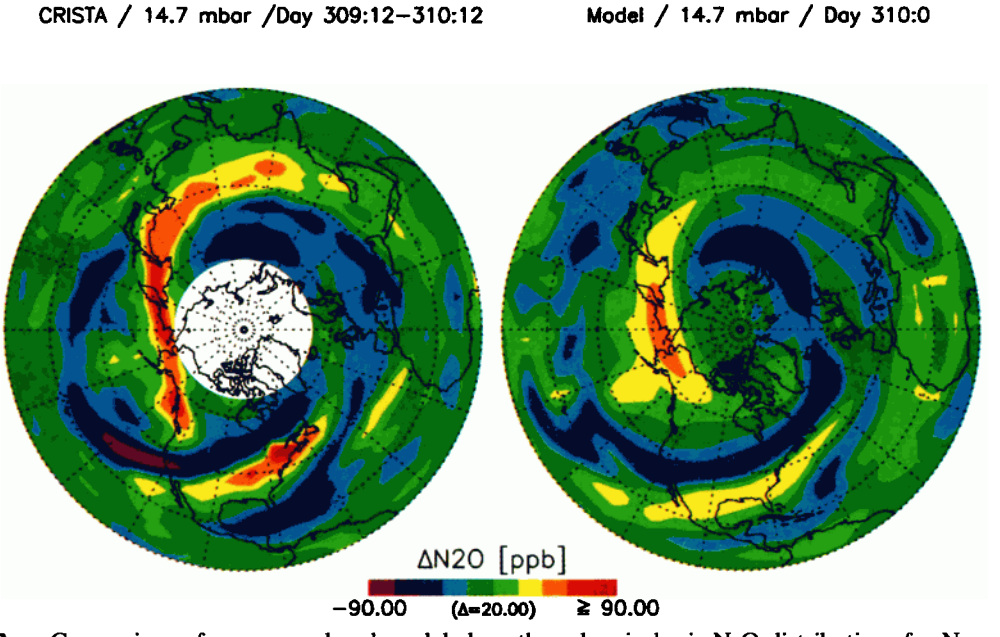

Plate 2a. Comparison of a measured and modeled northern hemispheric N_2O distributions for November 6, 1994, at 14.7 mbar. Absolute values are shown as well as "detrended" values obtained by subtracting zonal averages at each latitude. The measured distribution shown in this plate was obtained by interpolating CRISTA level 2 data onto the model grid (64 × 72). The interpolation has been performed by applying a two-dimensional weighting function, which resembles a triangle function with a half width of 8° in longitude and 4° in latitude. For comparison reasons, this filter was also applied to the modeled distributions. The distributions of Plates 3 to 7 were calculated using the same approach.

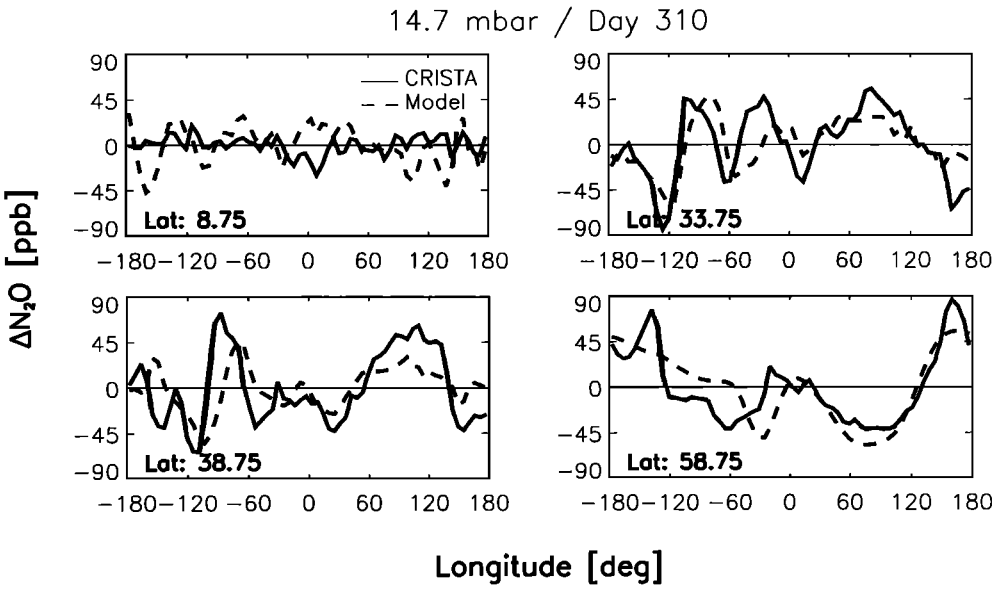

Plate 2b. Comparison of measured and modeled longitudinal cross sections of "detrended" N_2O values at 14.7 mbar. Data are shown at four latitudes of the model grid (8.75°, 33.75°, 38.75°, and 58.75°). The detrended values were obtained by subtracting zonal mean values at each latitude.

tures are more pronounced in the measured N_2O distribution at middle and high latitudes (see also Plate 2b).

In the tropics and subtropics the model results exhibit large medium-scale variability, which does not exist in the measured distribution. This discrepancy is shown in Plate 2b by means of longitudinal cross sections of detrended N_2O mixing ratios. At 8.75°N, unrealistically high variability is found in the model result. Since the structures of the modeled N_2O distribution are of medium scales, they would have been detected by CRISTA, if they were real. Such an overestimated variability in the tropics and subtropics appears to be a common problem of trace gas simulations based on assimilated winds. *Kindler et al.* [1998] find, for example, unrealistically large amplitudes of wavenumbers 4 to 7 in the tropics and subtropics when comparing N_2O simulations to Cryogenic Limb Array Etalon Spectrometer (CLAES) observations.

4. Temporal Development of Northern Hemispheric CFC-11 at 31.6 mbar

During the measurement period of CRISTA the shape of the north polar vortex varied significantly from day to day. A very pronounced planetary wave two structure (stretched vortex) decayed in favor of a planetary wave one structure (vortex shifted toward Scandinavia). Plate 3a shows a comparison of a measured and a modeled time sequence of CFC-11 distributions of the northern hemisphere (31.6 mbar) for the time period from November 6–10 (day 310 to day 314). Associated detrended CFC-11 mixing ratios (day 310 and day 312) are compared in Plate 3b at four different latitudes.

The calculated fields represent synoptic maps (e.g., day 310: 0), while the measured fields contain data that were measured within a 24 hours time period (e.g., from day 309:12 to day 310:12). The modeled distributions capture a lot of the dynamical features, especially at middle and high latitudes. On November 6 the deformation of the north polar vortex and the resulting pronounced wave two structure at high latitudes are indicated by CFC-11 poor vortex air. The north polar vortex is stretched toward Siberia and North America. The associated wind field advects air out of the tropics into higher latitudes. At this pressure level the strong tropical extrusion that extends across the United States into the Atlantic Ocean (see also Plate 2a) is most pronounced. The model reproduces this tropical extrusion well. During the following days the north polar vortex is shifted toward Europe, leading to a pronounced wave one structure. As a result, the extrusion of tropical air is also displaced toward the south and stretched toward Europe and Asia. The CFC-11 observations of day 314 suggest that some irreversible mixing of tropical air occurs over Europe and Asia.

The amplification of the wave one structure and the associated deformation of the tropical extrusion are very similar in both observation and simulation. However, minor differences of the transport processes show up in the comparisons of Plate 3b. On day 312 the modeled tropical extrusion is somewhat more shifted toward the south than the observed extrusion. As a result, a large discrepancy occurs in Plate 3b at 43.75°N. Notable differences between the observations and the model results also occur in the tropics and subtropics, where the model produces too much variability (see also section 3.2).

5. Trace Gas Assimilation

5.1. Sequential Technique

The good agreement between the model results and the measurements is very encouraging. The model has therefore been used as the core of a trace gas assimilation system. The aim of data assimilation is the construction of an optimum combination of a priori knowledge about a physical system (e.g., a model forecast) and observations of this system. For example, the UKMO data are an optimum combination of measured winds and temperatures and values provided by a general circulation model. The advantage of using assimilated stratospheric winds in constituent transport calculations has been first described by *Rood et al.* [1989]. However, for detailed

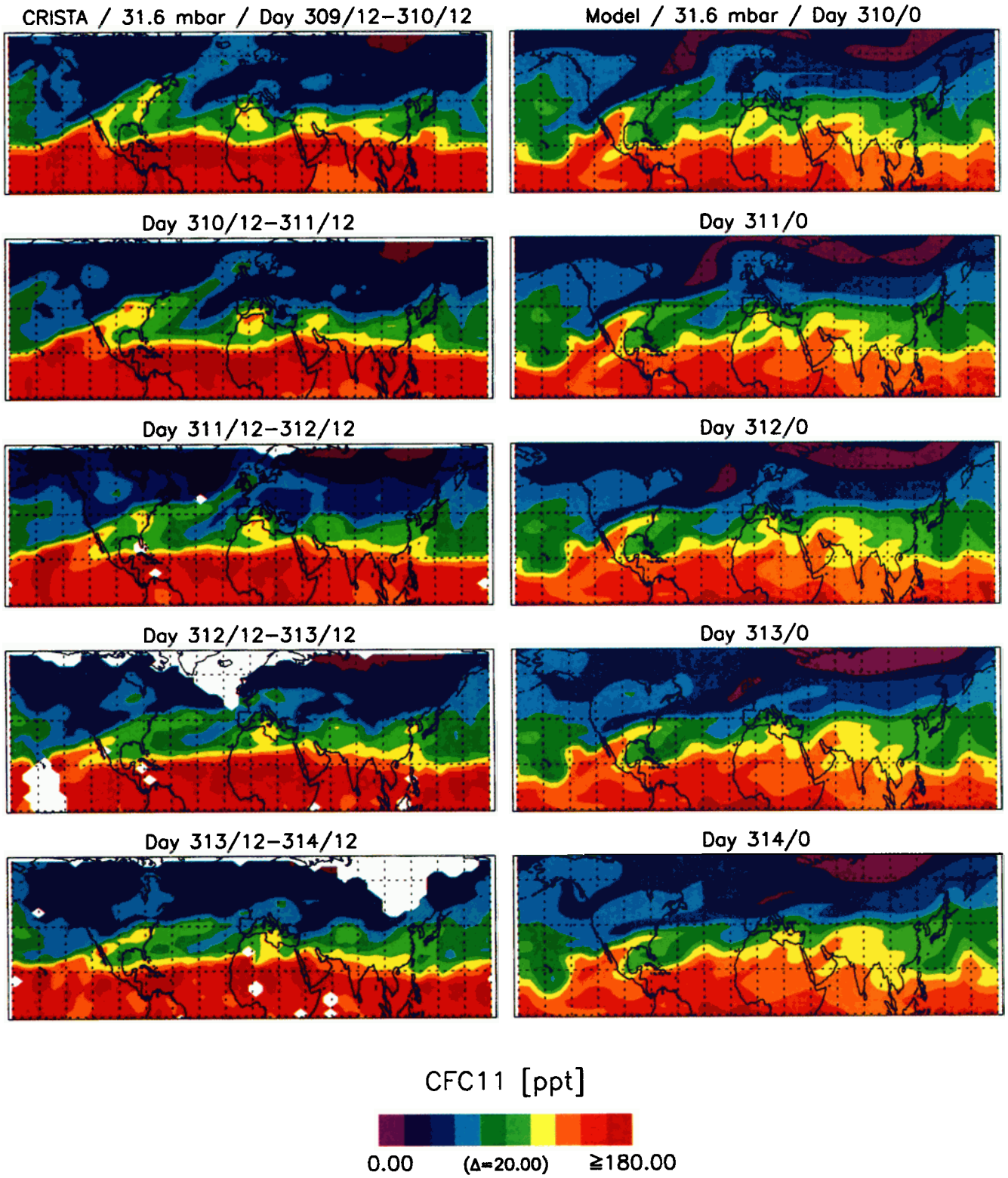

Plate 3a. Measured and modeled time sequence (November 6–10, 1994) of the northern hemispheric CFC-11 distribution at 31.6 mbar. Since CRISTA covers latitudes up to +67°, the data are compared in the latitudinal band from 0° to +70°. The blank areas in the measured maps indicate grid points where no measured data are available inside the nonzero region of the weighting function used for filtering the data.

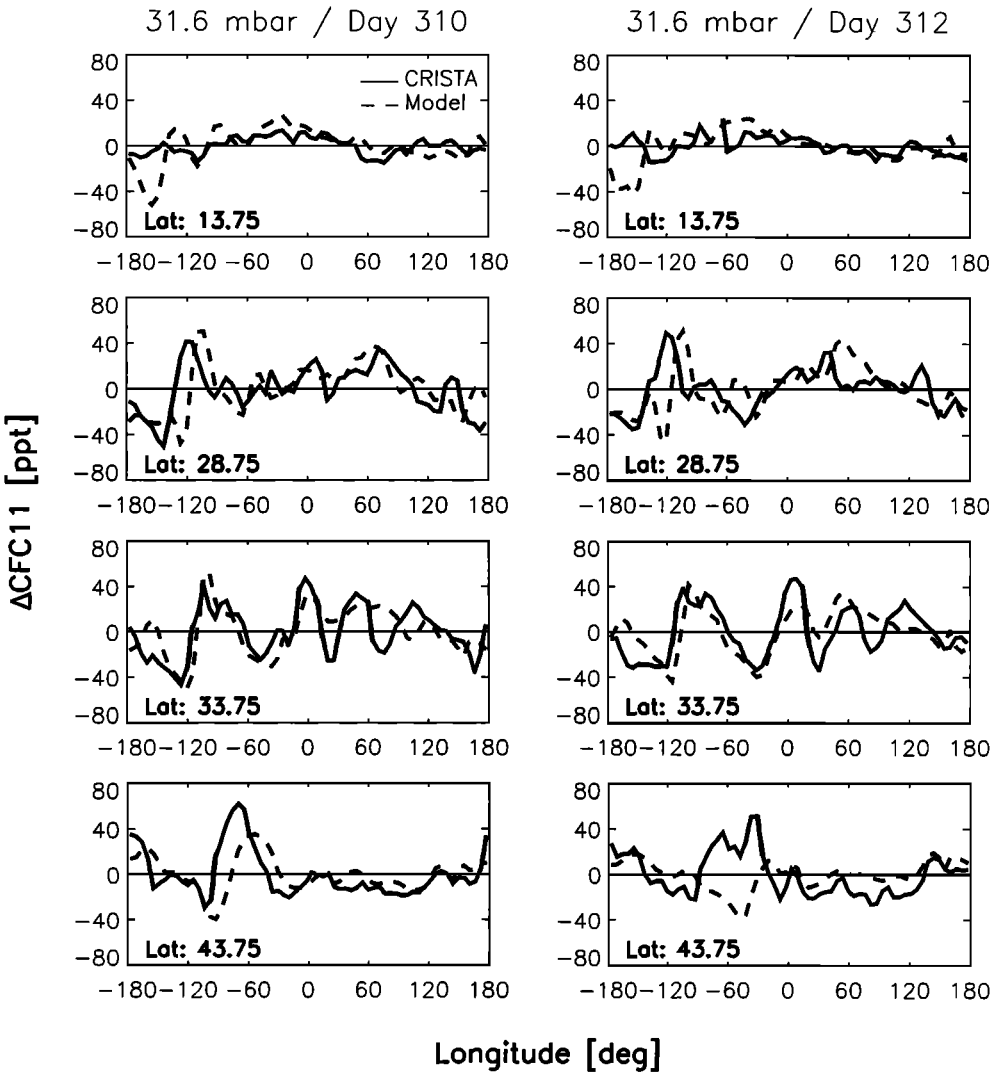

Plate 3b. Comparison of measured and modeled longitudinal cross sections of "detrended" CFC-11 values at 31.6 mbar for 2 days (November 6 and 8).

transport studies and for analyses of the interaction between transport and photochemistry, it is useful to assimilate the measured trace gas concentrations themselves in the model. A simple sequential assimilation technique was therefore used in order to combine version 1 level 2 data of CRISTA (instrument sampling grid) with trace gas fields provided by the ROSE model. This paper focuses on results obtained for long-lived tracers.

ROSE is initialized on November 1 (day 305:0) and calculates the synoptic evolution of the middle atmosphere. CRISTA measurements are available from November 4 (day 308:1735) on. After this date, the model is sampled by the measurement tracks of the three telescopes. At each time step, mixing ratio values calculated by the model are updated at all locations where measurements are available. By this approach the trace gas assimilation system accounts for the asynoptic nature of the CRISTA measurements.

Each measured value is used to update the model values at its four surrounding model grid points at the associated pressure level. The updates are weighted means of the measured value and the corresponding model forecasts. For each of the surrounding grid points the relative weight W of the measured value is calculated from its longitudinal ($\Delta\lambda$) and latitudinal ($\Delta\varphi$) distance as follows: $W = 1 - R$, $R = ((\Delta\lambda/\Delta\lambda_0)^2 + (\Delta\varphi/\Delta\varphi_0)^2)^{1/2}$, where $\Delta\lambda_0$ and $\Delta\varphi_0$ are the longitudinal and latitudinal resolution used for the model integration.

Because of the high data density of CRISTA, the distributions of long-lived trace gases are rapidly forced toward the observation, since all grid points are updated in about a day. After a transition phase, the model forecast essentially represents a temporal extrapolation of previous CRISTA measurements. As a result, the analyzed maps of long-lived tracers become rather insensitive to changes of the weighting factors applied to the measurements and to the model forecasts. In a sensitivity study performed for CFC-11 at 46.4 mbar, the weighting factor of the measurements was reduced by a factor of 2 after day 311:0. However, the resulting CFC-11 values of day 314:0 agree with the corresponding CFC-11 values of the standard approach typically within 5%.

The trace gas assimilation system provides synoptic (analyzed) maps at each time step (20 min) of the model. These analyzed maps are well suited for comparisons of CRISTA

trace gas observations and associated transport quantities to respective model results (without trace gas assimilation). In the analyzed maps, data gaps are filled by model predictions based on previous measurements, and the observations are extrapolated toward the poles.

5.2. Examples of Analyzed Maps

5.2.1. CFC-11 at 46.4 mbar. A comparison of measured and analyzed CFC-11 distributions is shown in Plate 4a for the time period from November 6–10 and the 46.4 mbar pressure level. The analyzed maps represent synoptic distributions of CFC-11 for 0000 UT each day, while the measured data corresponding to each map were gathered over a time span of 24 hours. There are some data gaps, especially on the last 2 days of the time sequence. This gaps are filled in the analyzed distributions by means of the model forecast which is based on previous observations.

There are interesting dynamical structures near 30°N latitude with a shape similar to Kelvin Helmholtz billows. The structure over the southern United States corresponds to the lower end of the tropical extrusion which has already been discussed in sections 3 and 4. On November 6 an air mass of relatively high CFC-11 mixing ratios, which is located south of Iceland, becomes separated from the tropical extrusion over the southern United States. During the following days this air parcel moves eastward and is somewhat stretched. The data suggest that irreversible mixing occurs. The south polar vortex is shifted toward South America throughout the measurement period of CRISTA. Its shape varies from day to day. On November 10 (day 314) a polar extrusion has developed. The associated wind field draws tropical air toward the south. The polar extrusion can only be seen in the analyzed distribution since the measured field exhibits a large data gap at this location (on this particular day). However, the southward transport of tropical air, which is a result of the interaction of the polar extrusion with tropical air, is also highlighted in the CRISTA measurements in the vicinity of the data gap.

The analyzed maps of Plate 4a can be considered as a value-added level 3 data product of CRISTA. In the standard data processing of CRISTA a Kalman filter is used which estimates amplitudes and phases of sinusoidal waves around the latitude circles in order to interpolate asynoptic level 2 data (instrument sampling grid) to synoptic grids (level 3 product). Zonal wavenumbers up to $m = 15$ are used for the Kalman filter [see *Offermann et al.*, this issue].

Plate 4b shows a comparison of the CFC-11 distribution (46.4 mbar) measured by CRISTA on November 7 with corresponding synoptic maps obtained from the assimilation (see Plate 4a), from the model, and from the Kalman filter ($m = 15$ and $m = 6$). The CFC-11 distributions are compared by means of scatterplots. In the case of the assimilation the scatter is about a factor of 1.5 smaller than in the case of the Kalman filter ($m = 15$). The scattering becomes much larger in the case of the Kalman filter of lower longitudinal resolution ($m = 6$) since the information contained in this synoptic field is equivalent to one viewing direction only. In the case of the model (see Plate 4b) the deviations are especially large for subtropical CFC-11 mixing ratio values (around 225 ppt).

The tendency of the model to produce unrealistic horizontal structures in the tropics and subtropics must also affect the assimilation, but to a much smaller degree, since new measurements are continually being inserted in the sequential assimilation procedure. From Plate 4b it can be concluded that there is no major impact on the analyzed CFC-11 distribution at 46.4 mbar. This is also confirmed by the histograms of Plate 4b, where percentage deviations of the analyzed field and of the Kalman field filtered ($m = 15$) field from the measurements for two latitudinal bands (0°N to 20°N and 20°N to 60°N) are shown.

5.2.2. N_2O at 10.0 mbar. A comparison of a measured, an assimilated, and a modeled N_2O distribution in the southern hemisphere (10 mbar) is shown in Plate 5 for November 6. The reproduction of the observation by the model is considerable worse than in the northern hemisphere (e.g., Plates 2a and 3a). As mentioned in section 1, the south polar vortex was already decaying at this pressure level. Obviously, the UKMO winds are not quite able to reproduce the complex pattern of the associated air motions (and the analyzed data are also affected by this). At longitudes of approximately 20°W, N_2O rich air is advected toward the south in both the model and the measurements. In the model there is a strong interaction of the elongated vortex with tropical air west of South America, while the vortex is more separated from the subtropics in the measured distribution. This is mainly due to the steeper horizontal gradient of the N_2O mixing ratio in the vicinity of the subtropical transport barrier. The most notable difference between the model and the measurements is the pronounced tongue of vortex air which is drawn out toward low latitudes. Over the Pacific Ocean the tongue extends along the −40° latitudinal circle. In reality, the wind field advects two weaker tongues along this latitudinal circle. One of these tongues originates from the edge of the polar vortex, while the other tongue contains air of relatively high N_2O mixing ratios.

To assess the effect of a different initial N_2O distribution, a zonally symmetric N_2O initialization was applied on November 1. On November 6, structures were found (not shown here) very similar to those of the modeled distribution of Plate 5.

5.2.3. N_2O and CH_4 at 4.6 mbar. The analyzed distributions are especially suited to study strong irreversible mixing processes that are evident in the tracer fields at higher altitudes. The temporal development of the analyzed N_2O and CH_4 distributions is shown in Plates 6 and 7 for the 4.6 mbar pressure level. As expected, structures in the distributions of both trace gases are well correlated, and the overall temporal evolution of the dynamics is reflected by both trace gases in a similar manner. On November 6 (day 310) an air mass of N_2O and CH_4 rich air is being separated from the air mass of the associated tropical extrusion (in the Atlantic off the coast of Nova Scotia). During the following days this air mass moves eastward and starts to circle around the north polar vortex. On November 12 (day 316) it is mixed into another air mass that extends along the Pacific coast. Parts of the large air mass of N_2O/CH_4 rich air which is located over the Pacific Ocean are drawn through the southern United States toward the Atlantic. During the following days there are complex interactions with the polar extrusions of N_2O/CH_4 poor air.

Randel et al. [1993] have used N_2O and H_2O concentrations provided by the UARS CLAES and Microwave Limb Sounder (MLS) instruments to analyze a similar tropical extrusion that occurred in early September 1992 over South America. They conclude that such episodic events could be responsible for a significant transport of stratospheric air across the tropical transport barrier. *Kindler et al.* [1998] have modeled this event using UKMO and NASA winds. However, these analyses provide a qualitative view on the associated transport and mixing processes only. The analyzed maps shown in Plates 6 and 7

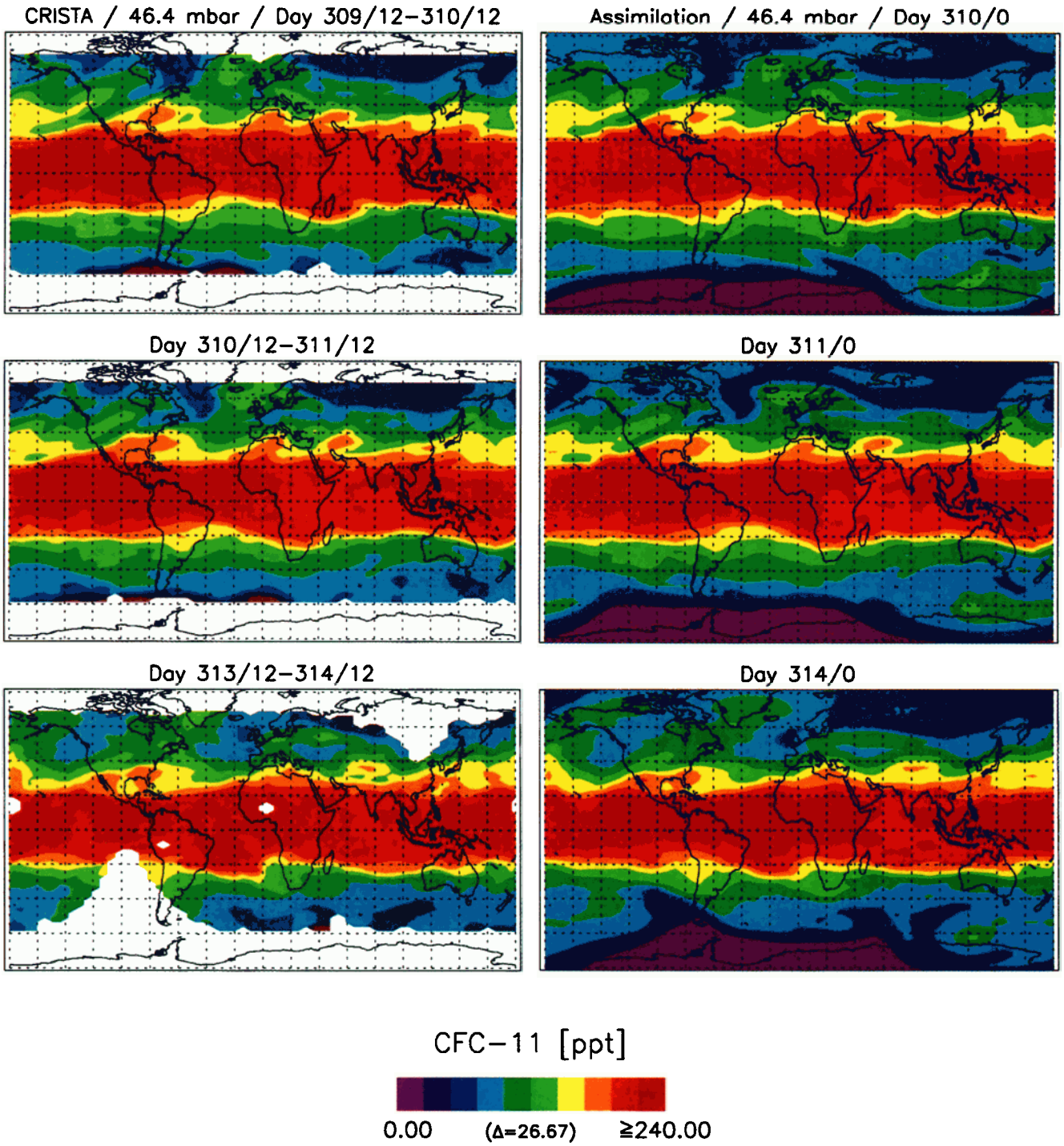

Plate 4a. Comparison of measured and analyzed CFC-11 maps at 46.4 mbar for November 6, 7, and 10, 1994. The measurements of each map were taken over 24 hours, while the analyzed data represent synoptic maps (0000 UT). Note the horizontal density of the measured data of day 314 is about a factor of 2 lower than on days 310 and 311. This is not apparent in the filtered data shown in this plate. Blank areas in the measured distributions have the same reason as in Plate 3a.

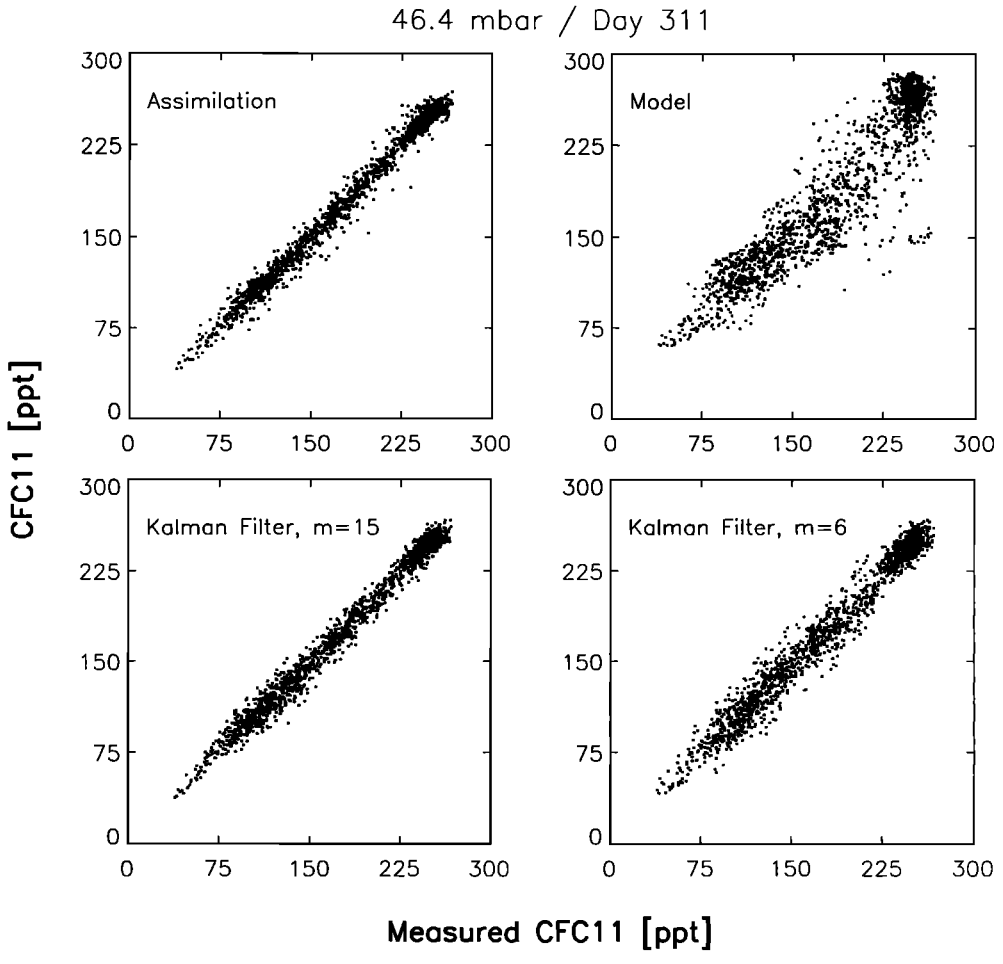

Plate 4b. Comparison of measured CFC-11 values (46.4 mbar, November 7) with corresponding synoptic distributions obtained from the assimilation (analyzed values), the model, and a Kalman filter ($m = 15$, $m = 6$).

allow for a more detailed quantitative study of the events that occurred during the time period of the CRISTA measurements.

In addition to examples of transport from the tropics into middle latitudes, which have also been shown in previous studies, the CRISTA data of Plates 6 and 7 indicate a pronounced transport in the opposite direction. In Plate 7 it can be seen that CH_4 poor air is transported from middle latitudes into the tropics at 40°N, 110°E (days 310 to 312). After November 8 (day 312), an air mass of relatively low CH_4 mixing ratios is located at 20°N, 90°E, and it is surrounded by air of higher mixing ratios. Thus the time sequence of the analyzed data suggests that irreversible mixing occurs.

6. Trace Gas Transport and Budgets

Quantitative analysis of the transport associated with the structures in the trace gas distributions measured by CRISTA (e.g., Plates 3a, 3b, and 7) can be performed by means of the transformed Eulerian-mean (TEM) conservation equation (equation (1)) for zonal mean mixing ratios [*Andrews et al.*, 1987]. This approach has also been used by *Randel et al.* [1994] for a study of the N_2O budget in the middle atmosphere version of the NCAR Community Climate Model (CCM2) [*Boville*, 1995].

$$\frac{\partial \bar{\chi}}{\partial t} = -\overline{v^*}\bar{\chi}_y - \overline{w^*}\bar{\chi}_z + \bar{S} + \frac{1}{\rho}\nabla \cdot \mathbf{M} \tag{1}$$

The quantity on the left side of (1) ($\partial\bar{\chi}/\partial t$) is the mixing ratio tendency. Forcing terms for (1) include advection represented here by the residual mean circulation ($\overline{w^*}$, $\overline{v^*}$), defined as

$$\overline{w^*} = \bar{w} + \frac{1}{a\cos\varphi}\frac{\partial}{\partial\varphi}\left(\cos\varphi\,\frac{R}{H}\,\frac{\overline{v'T'}}{N^2}\right) \tag{2}$$

$$\overline{v^*} = \bar{v} - \frac{1}{\rho}\frac{\partial}{\partial z}\left(\rho\,\frac{R}{H}\,\frac{\overline{v'T'}}{N^2}\right) \tag{3}$$

The source term $\bar{S}$ in (1) accounts for the photochemical production (and loss), and $\mathbf{M}$ is the eddy flux vector with horizontal and vertical components given by

$$M_y = -\rho\left(\overline{v'\chi'} - \frac{R}{H}\,\frac{\overline{v'T'}}{N^2}\,\bar{\chi}_z\right) \tag{4}$$

$$M_z = -\rho\left(\overline{w'\chi'} - \frac{R}{H}\,\frac{\overline{v'T'}}{N^2}\,\bar{\chi}_y\right) \tag{5}$$

Overbars denote zonal means. Primes denote deviations from the zonal mean values.

The analyzed CRISTA distributions (see section 5) are ide-

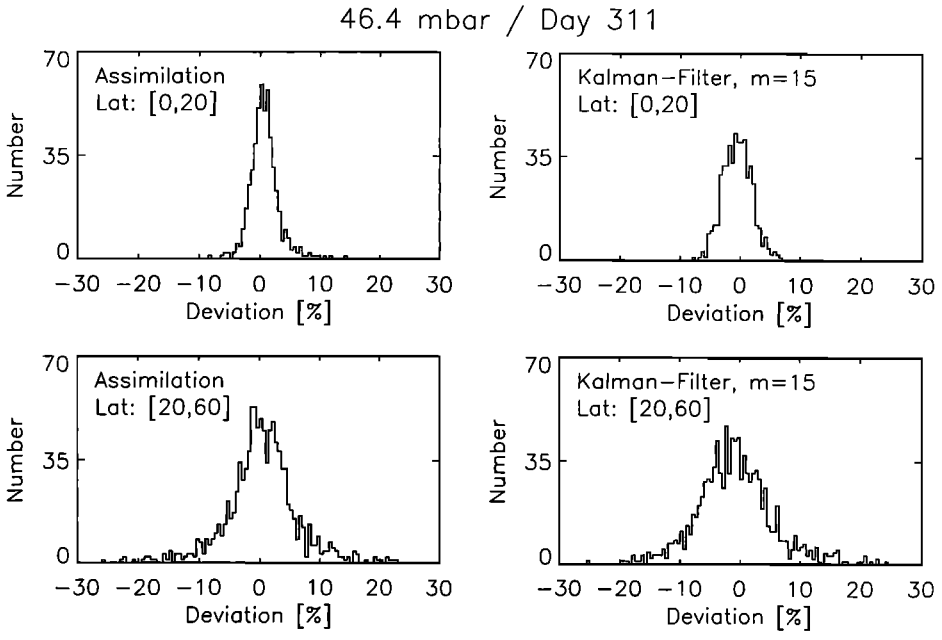

Plate 4c. Percentage deviations of measured CFC-11 values (46.4 mbar) from assimilated and Kalman-filtered (m = 15) values. The deviations are shown for two latitudinal bands (0° to 20°N and 20°N to 60°N) by means of histograms. The histograms show the number of points for a bin size of 1%.

ally suited for analyses of tranport processes based on (1) to (5) since all information needed to evaluate (1) to (5) is available at each time step in a consistent manner with the CRISTA trace gas measurements. Figure 1a compares the meridional CFC-11 eddy flux ($-(1/\rho)\,M_y$) at 31.6 mbar derived from the analyzed CRISTA measurements and from the UKMO winds and temperatures (solid curve) with the corresponding values provided by the model without data assimilation (dashed curve) for November 6 (day 310:0). The general meridional distribution of the CFC-11 fluxes is quite similar; however, the flux derived from the analyzed data is somewhat larger at middle latitudes.

Figure 1b shows mean CFC-11 eddy fluxes for the time period from day 310:0 to day 314:0 (same time period as in Plate 3a). The fluxes have been calculated with a temporal resolution of 1 day. Figure 1b shows averages of the values obtained for the single days. The mean flux of the model is somewhat overestimated in the equatorial region (due to the higher variability of the CFC-11 mixing ratios). It is smaller northward of about 30°N since the modeled structures are less pronounced at higher latitudes. In comparison to the single day observation (Figure 1a), the mean curves are flattened. This means that large parts of the CFC-11 mixing ratio tendencies associated with the fluxes of single days cancel when averaged over longer time periods. Note that *Randel et al.* [1994] also find a large degree of reversibility of transport effects during wave-disturbed periods in their analysis of CCM2 simulations.

The calculation of net trace gas tendencies is somewhat suffering from the short measurement period of CRISTA. The approach presented here is thus exploratory in nature. The budgets of two specific tracers, CFC-11 (31.6 mbar) and CH_4 (4.6 mbar), are studied. As will be shown below, net tendencies (left side of equation (1)) of CFC-11 (31.6 mbar) are of the order of 1 ppt/d during the measurement period of CRISTA. This corresponds to about 0.5%/d of the equatorial CFC-11 value only. Net tendencies of CH_4 at 4.6 mbar are somewhat larger. The calculation of transport terms (right side of equation (1)) is based on CRISTA trace gas structures and UKMO wind and temperature fluctuations obtained from synoptic fields. The accuracy of these quantities is not limited by the short measurement period of CRISTA. However, fluctuations obtained from different data sets have to be combined, and spatial derivatives have to be calculated.

Figure 2a compares net tendencies of CFC-11 at 31.6 mbar ($\partial\bar{\chi}/\partial t$, solid curve, hereafter measured tendencies) to tendencies calculated from transport terms on the right of (1). The measured tendencies have been determined by comparing zonal mean CFC-11 values of day 310:0 to respective values of day 314:0. The divergence of the eddy flux and the effects of the residual mean circulation have been calculated with a temporal resolution of 1 day. Figure 2a shows averages obtained for the time period from day 310:0 to 314:0. When comparing the measured to the calculated tendencies, there are latitudinal bands of qualitative agreement (20°N to 40°N) and latitudinal bands of qualitative disagreement (e.g., 0° to 20°N). The deviations between the measured and the calculated tendencies should be considered as the uncertainties of this budget analyses. This implies that the CFC-11 (31.6 mbar) results obtained at latitudes below 20°N are useless. However, in the latitudinal band from 20°N to 40°N the measured and the calculated tendencies are in reasonable agreement. Both curves exhibit two relative maxima (at 25°N and 40°N). The evaluation of the transport terms indicates that the maximum at 25°N results from the mean residual circulation (dash-dotted curve in Figure 2a), while the maximum at 40°N is an effect of eddy transport (dashed curve in Figure 2a).

Version 1 data of CRISTA contain CFC-11 values only above 20 km. However, the altitude range of CFC-11 will be extended down to 15 km in future data versions. Budget anal-

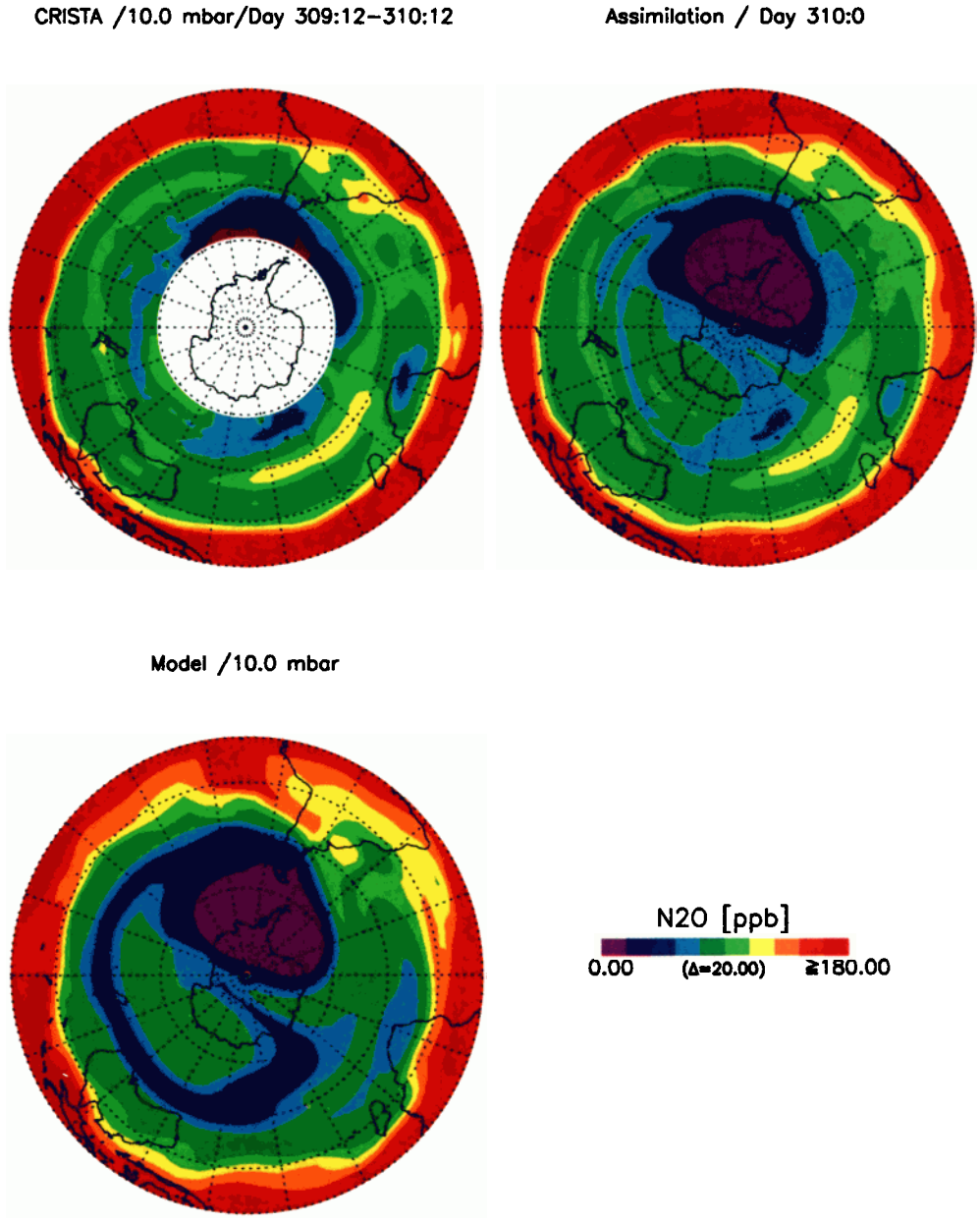

Plate 5. Comparison of a measured, an analyzed, and a modeled southern hemispheric distribution of N_2O for November 6, 1994, at 10 mbar.

ysis of these distributions might provide useful information on potential effects of stratospheric aircrafts flying at high altitudes.

Figure 2b compares measured CH_4 (4.6 mbar) tendencies ($\partial\bar{\chi}/\partial t$, solid curve) to tendencies calculated from the sum of all terms on the right of (1) at 4.6 mbar (see Plate 7). Effects of the eddy flux divergence ($(1/\rho)\nabla\mathbf{M}$, dashed curve) are much larger than effects of the residual mean circulation and of photochemical production and loss. Thus the results are not significantly affected by uncertainties of the reaction rate constants taken from *DeMore et al.* [1994]. In general, differences between measured and calculated tendencies are much smaller than in the case of CFC-11. Thus the analysis performed for CH_4 at 4.6 mbar appears to be more reliable. The relative latitudinal shape of the measured and the calculated tendencies is in reasonable agreement. This shape is a result of the eddy flux divergence (dashed curve in Figure 2b). The relative minimum at 20°N shows up in the measured tendencies as well as in the calculated tendencies. It is related to the transport process from middle latitudes to the tropics, which is discussed in section 5. Measured zonal mean mixing ratio tendencies are about −0.007 ppm/d at 18.75°N (Figure 2b). A longitudinal cross section at this latitude shows that the largest tendencies (−0.03 ppm/d) occur in a latitudinal band of about 50° centered around 80°E.

7. Summary and Discussion

High-resolution stratospheric CRISTA data of CFC-11, N_2O, and CH_4 have been compared and combined with respective trace gas fields simulated with the UKMO wind-driven version of the ROSE model. The wind fields are able to produce synoptic trace gas maps which are in good agreement with

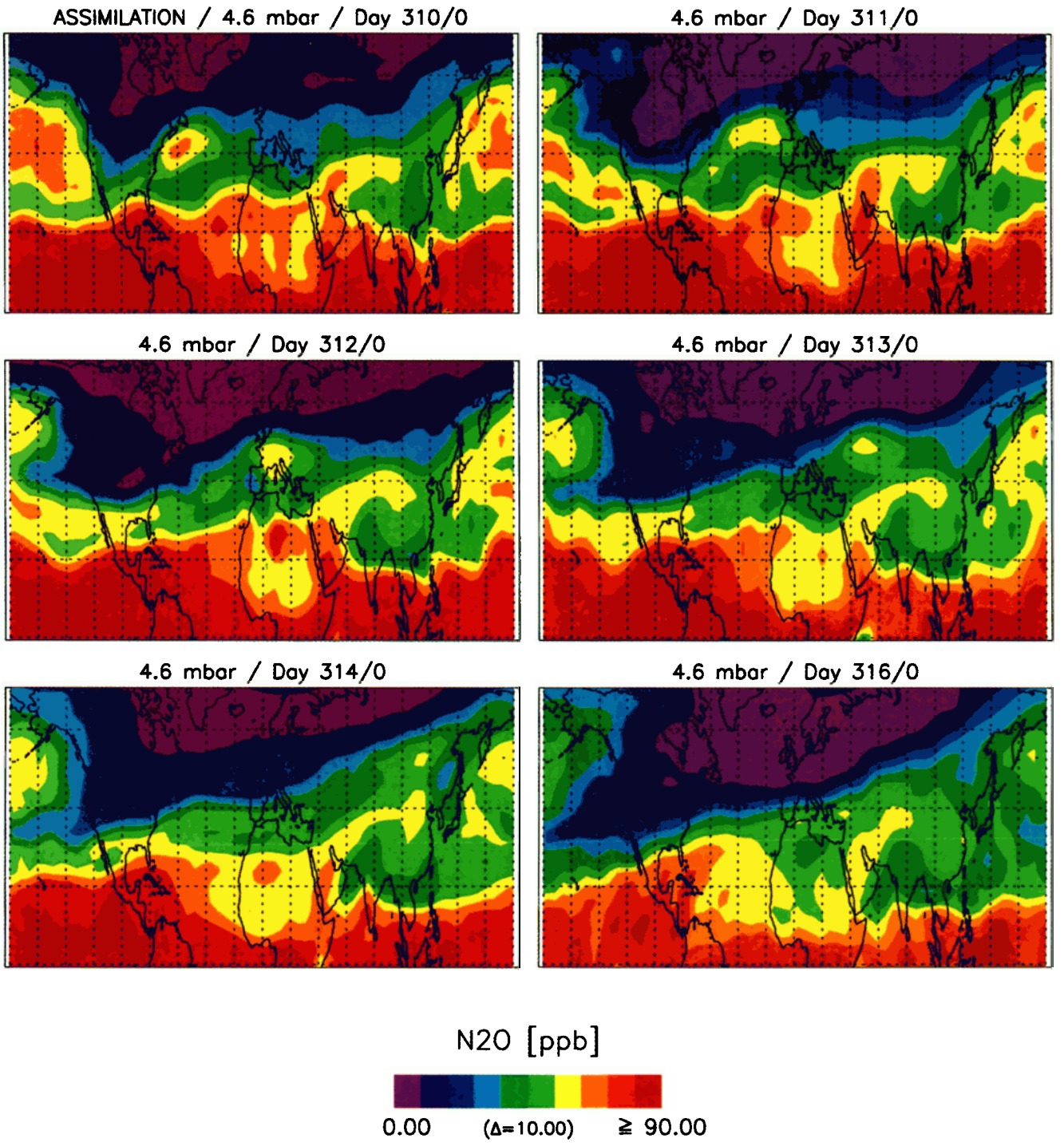

Plate 6. Time sequence of analyzed N_2O data of CRISTA at 4.6 mbar. Data are shown for November 6, 7, 8, 9, 10, and 12, 1994. (For details, see text.)

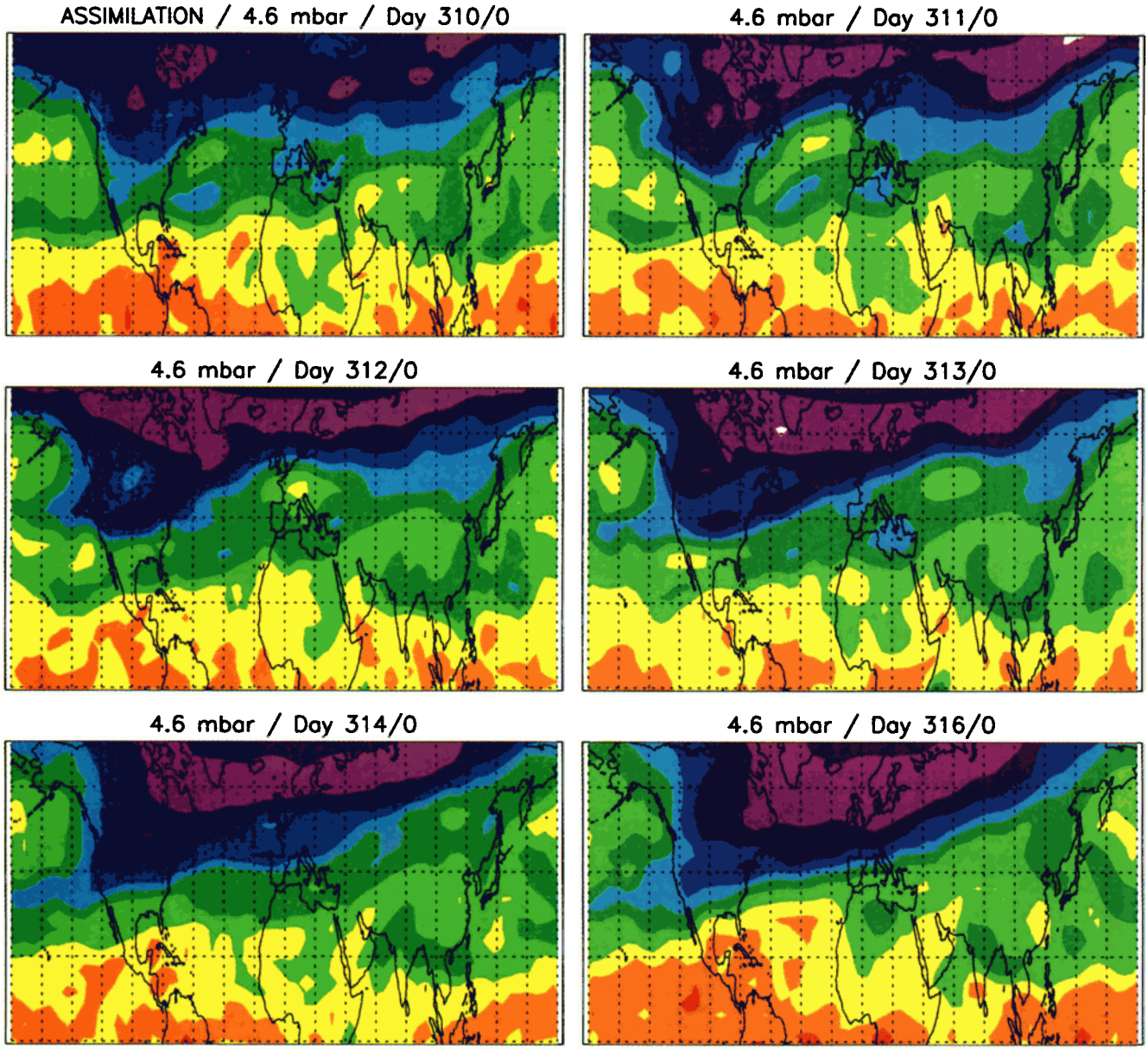

Plate 7. Same as in Plate 6, but for CH_4.

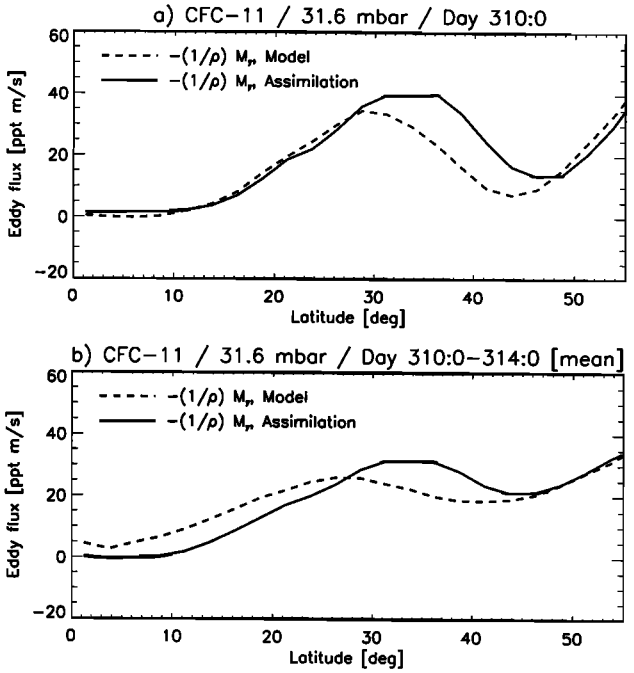

Figure 1. (a) Comparison of the meridional CFC-11 flux derived from analyzed CRISTA data (solid curve) for November 6 (day 310:0) at 31.6 mbar with the respective CFC-11 flux derived from model simulations without trace gas data assimilation (dashed curve). At 30°N the longitudinal interval of the subtropical extrusion (140°E to 120°E) contributes about 25% to the measured eddy flux (not shown here). (b) Same as in Figures 1a, but mean values for the time period from November 6–10 (day 310:0 to day 314:0).

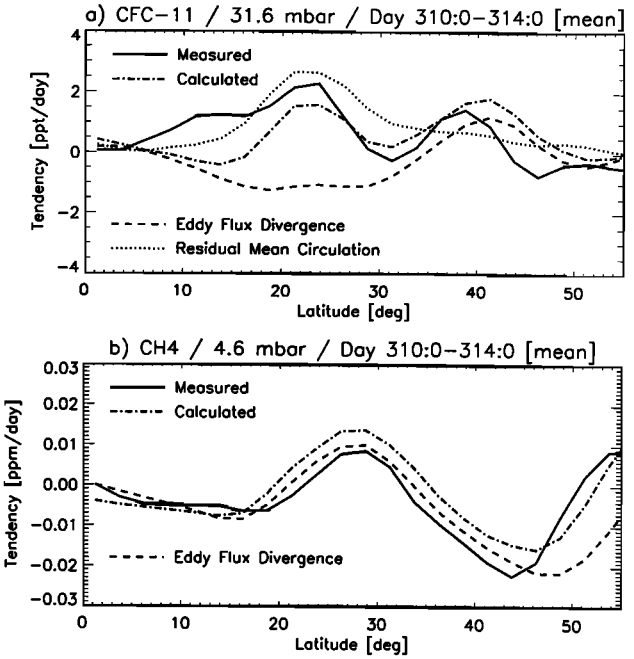

Figure 2. (a) Comparison of measured zonal mean tendencies of the CFC-11 mixing ratio (solid curve) at 31.6 mbar with transport-induced tendencies. The dotted curve represents the residual mean circulation. Effects of eddy transport are indicated by the dashed curve. The dash-dotted curve represents the sum of the transport effects. All values represent averages for the time period from November 6–10 (day 310:0 to day 314:0). (b) Comparison of measured zonal mean tendencies of CH_4 mixing ratios (solid curve) with calculated tendencies. The calculation includes all terms from the right side of equation (1). In addition, effects of eddy transport are shown by the dashed curve.

CRISTA measurements (e.g., Plates 2a and 3a). Some limitations apply, especially for the southern hemisphere (see Plate 5). The best agreement is found in the lower northern hemispheric stratosphere; however, the model produces unrealisticly high variability at equatorial and subtropical latitudes (e.g., Plates 2a and 2b). This appears to be a common problem of trace gas simulations based on assimilated meteorological data sets [see also *Kindler et al.*, 1998].

The CRISTA trace gas distributions have been combined with the ROSE model by using a simple assimilation technique which essentially interpolates the distributions of long-lived tracers measured by CRISTA onto the model grid used in this analysis. The assimilation system yields synoptic distributions that are consistent with the CRISTA measurements at each time step of the model (20 min). Data gaps are filled, and the measured trace gas distributions are extrapolated toward higher latitudes (see Plate 4a). The resulting analyzed trace gas fields can be considered as a value-added level 3 data product of CRISTA. They are especially suited to study temporal developments including small- and medium-scale transport and mixing processes. Meridional CFC-11 eddy fluxes at 31.6 mbar derived from analyzed CRISTA trace gas fields and UKMO winds are in reasonable agreement with eddy fluxes provided by model simulations without trace gas assimilation (see Figure 1). Both data sets indicate a large degree of reversibility of eddy transport at this altitude during the dynamically active period when CRISTA was operating [see also *Randel et al.*, 1994].

Irreversible processes are evident at higher altitudes (4.6 mbar). High-resolution measurements such as shown in Plates 6 and 7 provide a clear picture of transport processes including tropical/extratropical exchange of air masses. Most interesting is the mixing event from middle latitudes into the tropics that is shown in Plates 6 and 7 by means of analyzed N_2O and CH_4 concentrations. This event also shows up in the measured and calculated zonal mean tendencies of the CH_4 mixing ratio at around 20°N (Figure 2b).

The usefulness of CRISTA data for trace gas budget studies is somewhat limited by the relatively short measurement period of the instrument. However, the results shown in this paper demonstrate the great potential of using measured high-resolution trace gas fields in conjunction with a three-dimensional chemical transport model that is driven by assimilated wind and temperature fields. Long-term observations are expected to be provided, for example, by the High Resolution Dynamics Limb Sounder (HIRDLS) instrument on the EOS Chemistry Mission (CHEM) platform. Such observations will offer an unique opportunity to study seasonal cycles of transport processes and transported quantities in detail.

Acknowledgments. The authors wish to thank W. Randel, A. K. Smith, and B. Khattatov for helpful discussions. They acknowledge the contribution of A. Franzen and V. Kuell in the retrieval of CFC-11, N_2O, and CH_4. They also thank all other members of the CRISTA data analyses team for their efforts. The CRISTA project was supported by grant 50 OE 8503 of Deutsche Agentur fuer Welrauman-

gelegenheiten (DARA), Bonn, Germany. The CRISTA instrument was flown as part of the ATLAS 3 mission of the National Aeronautics and Space Administration (NASA), United States. The work of X. Tie is supported by the DOE Atmospheric Chemistry Program under contract DE-AI05-94ER619577. The National Center for Atmospheric Research is sponsored by the National Science Foundation.

References

Andrews, D. J., J. R. Holton, and C. B. Leovy, *Middle Atmosphere Dynamics, Int. Geophys. Ser.*, 489 pp., Academic, San Diego, Calif., 1987.

Bacmeister, J. T., V. Kuell, D. Offermann, M. Riese, and J. W. Elkins, Intercomparison of satellite and aircraft observations of ozone, CFC-11, and NO_y using trajectory mapping, *J. Geophys. Res.*, this issue.

Boville, B. A., Middle atmosphere version of community climate model, 2, Annual cycle and interannual variability, *J. Geophys. Res.*, *100*, 9017–9040, 1995.

Brasseur, G., M. H. Hitchman, S. Walters, M. Dymek, E. Falise, and M. Pirre, An interactive chemical dynamical radiative two-dimensional model of the middle atmosphere, *J. Geophys. Res.*, *95*, 5639–5655, 1990.

Chen, P., J. R. Holton, A. O'Neill, and R. Swinbank, Quasi-horizontal transport and mixing in the Antarctic stratosphere, *J. Geophys. Res.*, *99*, 16,851–16,866, 1994.

Chipperfield, M., Multiannual simulations with a three-dimensional chemical transport model, *J. Geophys. Res.*, *104*, 1781–1806, 1999.

DeMore, W. B., S. P. Sanders, D. M. Golden, R. F. Hampson, M. J. Kurylo, C. J. Howard, A. R. Ravishankara, C. E. Kolb, and M. J. Molina, Chemical kinetics and photochemical data for use in stratospheric modeling, *JPL Publ.*, *94-26*, 1994.

Douglass, A. R., C. J. Weaver, R. B. Rood, and L. Coy, A three-dimensional simulation of the ozone annual cycle using winds from a data assimilation system, *J. Geophys. Res.*, *101*, 1463–1474, 1996.

Garcia, R. R., F. Stordal, S. Solomon, and J. T. Kiehl, A numerical model of zonally averaged dynamical and chemical structure in the middle atmosphere, *J. Geophys. Res.*, *97*, 12,967–12,991, 1992.

Granier, C., and G. Brasseur, Ozone and other trace gases in the Arctic and Antarctic regions: Three-dimensional model simulations, *J. Geophys. Res.*, *96*, 2995–3011, 1991.

Holton, J. R., and W.-K. Choi, Transport circulation deduced from SAMS trace specie data, *J. Atmos. Sci.*, *45*, 1929–1939, 1988.

Kaye, J. A., and T. Miller, The ATLAS series of shuttle missions, *Geophys. Res. Lett.*, *23*, 2285–2288, 1996.

Kindler, T. P., D. M. Cunnold, F. N. Alyea, W. L. Chameides, G. P. Lou, and K. Schwan, An evaluation using ^{14}C and N_2O simulations of three-dimensional transport driven by United Kingdom Meteorological Office and Goddard Space Flight Center assimilated winds, *J. Geophys. Res.*, *103*, 10,827–10,847, 1998.

Kouker, W., D. Offermann, V. Kuell, R. Ruhnke, T. Reddmann, and A. Franzen, Streamers observed by the CRISTA experiment and simulated in the KASIMA model, *J. Geophys. Res.*, this issue.

Lary, D. J., M. P. Chipperfield, J. A. Pyle, W. A. Norton, and L. Riishojguard, Three dimensional tracer initialization and general diagnostics using equivalent PV-latitude-potential temperature coordinates, *Q. J. R. Meteorol. Soc.*, *121*, 187–210, 1995.

Lefèvre, F., G. P. Brasseur, I. Folkin, A. K. Smith, and P. Simon, Chemistry of the 1991–1992 stratospheric winter: Three-dimensional model simulations, *J. Geophys. Res.*, *99*, 8183–8195, 1994.

Mahlman, J. D., H. Levy II, and W. J. Moxim, Three-dimensional simulations of stratospheric N_2O: Predictions for other trace constituents, *J. Geophys. Res.*, *91*, 2687–2707, 1986.

Manney, G. L., R. Swinbank, and A. O'Neill, Stratospheric meteorological conditions from the November 3–12, 1994, ATMOS/ATLAS 3 measurements, *Geophys. Res. Lett.*, *23*, 2409–2412, 1996.

McIntyre, M. E., and T. N. Palmer, Breaking planetary waves in the stratosphere, *Nature*, *305*, 593–600, 1983.

Naujokat, B., and S. Pawson, The cold stratospheric winters 1994/1995 and 1995/1996, *Geophys. Res. Lett.*, *23*, 3703–3706, 1996.

Offermann, D., K. U. Grossmann, P. Barthol, P. Knieling, M. Riese, and R. Trant, The Cryogenic Infrared Spectrometers and Telescopes for the Atmosphere (CRISTA) experiment and middle atmosphere variability, *J. Geophys. Res.*, this issue.

Randel, W. J., J. C. Gille, A. E. Roche, J. B. Kumer, J. L. Mergenthaler, J. W. Waters, E. F. Fishbein, and W. A. Lahoz, Stratospheric transport from the tropics to middle latitudes by planetary wave mixing, *Nature*, *365*, 533–535, 1993.

Randel, W. J., B. A. Boville, J. C. Gille, P. L. Bailey, S. T. Massie, J. B. Kumer, J. L. Mergenthaler, and A. E. Roche, Simulation of stratospheric N_2O in the NCAR CCM2: Comparison with CLAES data and global budget analysis, *J. Atmos. Sci.*, *51*, 2834–2845, 1994.

Reber, C. A., Upper Atmosphere Research Satellite (UARS) mission, *NASA Rep.*, *430-1003-001*, 1985.

Riese, M., P. Preusse, R. Spang, M. Ern, M. Jarisch, K. U. Grossmann, and D. Offermann, Measurements of trace gases by the Cryogenic Infrared Spectrometers and Telescopes for the Atmosphere (CRISTA) experiment, *Adv. Space Res.*, *19*, 563–566, 1997.

Riese, M., R. Spang, P. Preusse, M. Ern, M. Jarisch, D. Offermann, and K. U. Grossmann, Cryogenic Infrared Spectrometers and Telescopes for the Atmosphere (CRISTA) data processing and atmospheric temperature and trace gas retrieval, *J. Geophys. Res.*, this issue.

Rood, R. B., D. J. Allen, W. E. Baker, D. J. Lamich, and J. A. Kaye, The use of assimilated stratospheric data in constituent transport calculations, *J. Atmos. Sci.*, *46*, 687–701, 1989.

Rood, R. B., E. Nielsen, R. Stolarski, A. Douglass, J. Kaye, and D. J. Allen, Episodic total ozone minima and associated effects on heterogeneous chemistry and lower stratospheric transport, *J. Geophys. Res.*, *97*, 7979–7996, 1992.

Rose, K., On the influence of nonlinear wave-wave interactions in a 3-D primitive equation model for sudden stratospheric warmings, *Contrib. Atmos. Phys.*, *56*, 14–41, 1983.

Rose, K., and G. Brasseur, A three-dimensional model of chemically active trace species in the middle atmosphere during disturbed winter conditions, *J. Geophys. Res.*, *94*, 16,387–16,403, 1989.

Rosenlof, K. H., and J. R. Holton, Estimates of the stratospheric residual circulation using the downward control principle, *J. Geophys. Res.*, *98*, 10,456–10,479, 1993.

Schoeberl, M. R., L. R. Lait, P. A. Newman, and J. E. Rosenfield, The structure of the polar vortex, *J. Geophys. Res.*, *97*, 7859–7882, 1992.

Smith, A. K., Numerical simulations of global variations of temperature, ozone, and trace species in the stratosphere, *J. Geophys. Res.*, *100*, 1253–1269, 1995.

Smolarkiewicz, P. K., and P. J. Rasch, Monotone advection on the sphere: An Eulerian versus semi-Lagrangian approach, *J. Atmos. Sci.*, *48*, 793–810, 1991.

Solomon, S., J. T. Kiehl, R. R. Garcia, and W. Grose, Tracer transport by the diabatic circulation deduced from satellite observations, *J. Atmos. Sci.*, *43*, 1603–1617, 1986.

Stanford, J. L., J. R. Ziemke, and S. Y. Gao, Stratospheric circulation features deduced from SAMS constituent data, *J. Atmos. Sci.*, *50*, 226–246, 1993.

Suarez, M. J., S. Schubert, A. Molod, C. Park, L. Takacs, C. Wu, M. Seabloom, W. Higgins, R. Rood, and Y. Kondratyeva, A multi year assimilation with the GEOS-1 system: Overview and results, *NASA Tech. Memo.*, *104606*, 1995.

Swinbank, R., and A. O'Neill, A stratosphere-troposphere data assimilation system, *Mon. Weather Rev.*, *122*, 686–702, 1994.

G. Brasseur and X. Tie, National Center for Atmospheric Research, Boulder, CO 80307.

D. Offermann and M. Riese, Physics Department, University of Wuppertal, Gauss-Str. 20, Wuppertal D-42097, Germany. (riese@wpos2.physik.uni-wupertal.de)

(Received December 14, 1998; revised March 15, 1999; accepted March 16, 1999.)